2001 IEEE/ASME International Conference on
Advanced Intelligent Mechatronics Proceedings
8—12 July 2001 • Como, Italy

Coulomb and viscous friction fault detection with application to a pneumatic actuator

W.B. Dunbar, R.A. de Callafon and J.B. Kosmatka

University of California, San Diego
Dept. of Mechanical and Aerospace Engineering
9500 Gilman Drive, La Jolla, CA 92093-0411, U.S.A
dunbar@cds.caltech.edu, {callafon,jkosmatk}@ucsd.edu

Abstract— **Generally, fault detection is the process of monitoring a physical dynamic system accompanied by confirmation and assessment of any degradation of system performance. These systems are modelled and terms that are representative of a specific fault are identified and monitored for detection. In this paper, a fault detection algorithm is developed to isolate and detect friction changes in a high precision positioning mechanism. The designed fault detection algorithm addresses dynamic model estimation, dynamic filtering and recursive parameter estimation techniques to monitor on-line friction changes. The procedure is illustrated on a high precision servo pneumatic cylinder that drives a translational air bearing apparatus, designed to permit the addition of friction. Side loading of the cylinder rod induced by a friction fault causes significant loss of performance in these applications. It therefore serves to design a simple and effective on-line fault detection and isolation scheme for the designed experimental set-up.**

I. Introduction

A characterization of external friction disturbances is beneficial for servo control applications where high precision positioning is crucial. The adverse effects of friction can be controlled by friction compensation [1], for which a characterization of the friction is required. In this paper, a friction fault detection algorithm is designed to monitor friction changes in a mechanical positioning mechanism. The algorithm proposed in this paper is able to monitor Coulomb and viscous friction separately by an on-line estimation of the friction parameters. The on-line detection of friction (fault) presented in this paper could facilitate the compensation of dry friction in high precision positioning mechanisms. Moreover, a fault detection technique for monitoring dry friction would help the detection of changing process conditions.

The friction detection technique developed in this paper is designed and illustrated on a servo pneumatic cylinder that drives an air bearing mass load. The air bearing mass is configured in such a way that it allows for (sudden) changes in the friction conditions. The friction fault detection scheme is implemented by simply adding an acceleration sensor to the load of the pneumatic cylinder. As a result, the scheme does not require the use of any type of compensation and is therefore independent of the control strategy implemented for these types of applications. Several experimental test cases prove that the scheme is successful.

The paper is organized as follows. The experimental set-up for the friction detection algorithm is described in Section II. The subsequent sections contain the key steps in the generation of the friction fault detection scheme. First, the dynamic modelling based on parametric identification of the pneumatic actuator and servo valve is discussed in Section III. Section IV presents the friction fault detection algorithm, where parameters in a proposed friction model are estimated recursively. The implementation results are detailed in Section V and conclusions are given in Section VI.

W.B. Dunbar is currently a doctoral student in the Control and Dynamical Systems department at the California Institute of Technology.

R.A. de Callafon is an Assistant Professor in the department of Mechanical and Aerospace Engineering at UCSD.

J.B. Kosmatka is a Professor in the department of Structural Engineering at UCSD.

II. Case study: pneumatic actuator

Pneumatic actuators (cylinders) are air driven actuation devices, where the air is regulated by some type of voltage controlled valve [2]. These actuators are in increasing use in industry in electro-mechanical systems with precision positioning objectives [3], [4], [5]. The presence of Coulomb friction in these actuators is a chief obstacle in automated systems that require precision positioning. This dry friction phenomena can interfere with the precision positioning objectives and cause problems like overshooting and force limit-cycling [6].

A schematic of the experimental precision positioning apparatus used in this paper is given in Figure 1. The

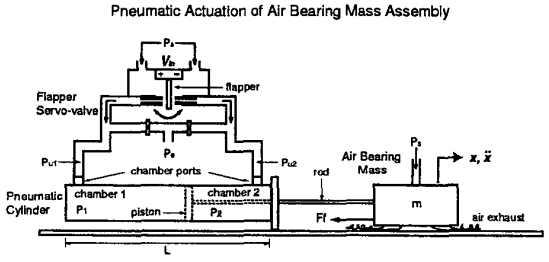

Fig. 1. Experimental Apparatus of an Air Bearing Mass with Pneumatic Actuation.

voltage V_{in} supplied to the flapper servo-valve directs the flapper and hence the flow of air to the two piston chambers. Asymmetric flow, i.e. nonzero valve voltage, ultimately creates a pressure difference in the cylinder chambers and the piston, rod and air bearing mass are forced into motion. The air bearing mass is designed to permit the addition of dry friction on-line. The mass is two hollowed out sections of aluminum block bolted together with a supply hose port in the top section and 36 small exhaust holes in the bottom section. The block hovers on air as long as sufficient air is supplied to it (approximately 10 psi). The measured signals of interest for identification and detection

0-7803-6736-7/01/$10.00 © 2001 IEEE

are the voltage input V_{in} to the servo-valve and the acceleration $\ddot{x}$ of the air bearing mass. Mounted on the mass are an accelerometer for measuring $\ddot{x}$ and a linear variable differential transformer (LVDT) opposite the cylinder rod for measuring x (not shown in Figure 1. The mass rides above a levelled smooth aluminum surface with an exhaust channel cut in the direction of motion to escape the airflow. This channel enables a smooth transition to friction as the supply pressure is reduced below critical (contact) pressure. The height of the cylinder is set to thread the rod into the mass when the mass is exhausting enough air to make no contact with the level surface. Therefore, side loading of the rod is present when contact is induced and as it increases.

III. Dynamic modelling of the pneumatic actuator and servo valve

A. Experiment based modelling

For the modelling of the dynamical behavior of the pneumatic actuator with the flapper servo valve depicted in Figure 1, an experiment based modelling approach is used. The experiment based modelling approach in this paper uses system identification to experimentally model the dynamics from the valve voltage input V_{in} to the acceleration $\ddot{x}$ of the air bearing mass. The result is a linear dynamic time invariant model of the actuator that will be used in the monitoring of the coulomb and viscous friction on the basis of simple acceleration measurements of the system. Although the system is nonlinear, the LTI model suffices to this end under a wide range of operating conditions.

The experimental based modelling of the pneumatic actuator and the servo valve consists of two steps. First, an experiment design for data acquisition has to be performed. Subsequently, a parametric model estimation is carried out. The resulting dynamic model that relates the voltage input V_{in} of the valve to the acceleration $\ddot{x}$ of the mass is estimated on the basis of frequency domain measurements obtained from the experiment design.

B. Experimental data acquisition

For the experiment design, a chirp signal with an amplitude of 0.7 V over a frequency range between 0 and 20 Hz was used as an input signal for the valve voltage V_{in}. Both the position and the acceleration of the air bearing mass were measured under a low friction load regime (no friction fault) to model the pneumatic positioning mechanism without friction errors. For identification purposes, the dynamic relation between voltage input V_{in} of the valve and the acceleration $\ddot{x}$ of the mass is of importance. Additional position measurements were carried out to validate the model being estimated.

By means of spectral analysis [7], the frequency response between voltage input V_{in} of the valve and the acceleration $\ddot{x}$ of the mass is estimated. The estimated frequency response is denoted by $G(\omega)$ and Figure 2 shows a Bode plot of the estimated frequency response.

By inspection of Figure 2 it can be seen that the relation between voltage input V_{in} of the valve and the acceleration $\ddot{x}$ of the mass is a basic differentiator with a roll-off at approximately 10 Hz. The differentiating action is due to the proportional relation between valve voltage input and air flow at frequencies less than 10 Hz, where air flow is in turn proportional to load velocities. The roll-off frequency at 10 Hz is due to the valve dynamics as the flow controlled flapper in the valve behaves like a damped beam with a bandwidth of 10 Hz. For frequencies above 10 Hz, the valve saturates and the up stream pressures, and therefore the chamber pressures, remain essentially constant. Therefore, for voltage inputs that exceed 10 Hz, little motion in the pneumatic cylinder piston and the air bearing load is observed.

Taking into account these observations and the shape of the measured frequency response with the additional time delays that cause additional phase shifts, a relative simple

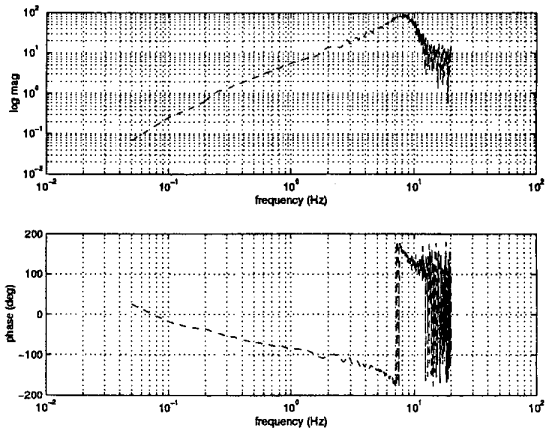

Fig. 2. Amplitude and Phase Bode Plot of the Frequency Response $G(\omega)$ that relates valve voltage input to air bearing mass acceleration

model with fourth order dynamics should be able to fit this frequency response. The result of the parametric identification of a fourth order model are given in the following section.

C. Parametric estimation of dynamic model

To model the dynamics between voltage input V_{in} of the valve and the friction free acceleration $\ddot{x}$ of the mass, a dynamic discrete time model $\hat{G}$ is being estimated. The discrete time model $\hat{G}$ is found by curve fitting the measured frequency response $G(\omega)$ given in Figure 2. During the curve fitting of the frequency response, the discrete time model is parameterized via a fourth order model

$$\begin{gathered}\hat{G}(q,\theta) = \frac{B(q,\theta)}{A(q,\theta)}, \text{ with} \\ B(q,\theta) = b_1 q^{-1} + b_2 q^{-2} + b_3 q^{-3} + b_4 q^{-4} \\ A(q,\theta) = 1 + a_1 q^{-1} + a_2 q^{-2} + a_3 q^{-3} + a_4 q^{-4} \\ \text{and } \theta = [b_1\ b_2\ b_3\ b_4\ a_1\ a_2\ a_3\ a_4]\end{gathered} \tag{1}$$

where q^{-1} denotes the usual shift operator $u(t-1) = q^{-1}u(t)$. The transfer function of the discrete time model $\hat{G}$ is given by $\hat{G}(z,\theta)$ with $z = e^{j\omega T}$, where T denotes the sampling time of the discrete time model $\hat{G}(z,\theta)$.

The 8 coefficients of the parameter θ are determined by means of a (non-linear) least squares curve fitting problem

$$\hat{\theta} = \arg\min_{\theta} \left\| \left[\hat{G}\left(e^{j\omega T}, \theta\right) - G(\omega) \right] W(\omega) \right\|_2 \tag{2}$$

where $G(\omega)$ is the measured frequency response data and $W(\omega)$ denotes an additional (frequency dependent) weighting function. The computational procedure to obtain θ is done with the frequency domain model identification program *FREQID* [8], [9]. The interface allows a weighting function $W(\omega)$ and model order selection during the estimation of a parametric model.

With FREQID, the model (1) is estimated using a weighting function $W(\omega) = |G(\omega)|^{-1}$ and a sample time $T = 1/256$ sec. The weighting function $W(\omega)$ is set to the inverse of the data $G(\omega)$ to minimize a relative error in (2). The sampling frequency of 256 Hz is chosen to accommodate the signal processing hardware on which the friction

nted. Note that a sampling frequency of 256 Hz captures all of the necessary dynamics of the system, as magnitude roll-off occurs well below the Nyquist frequency of 128 Hz.

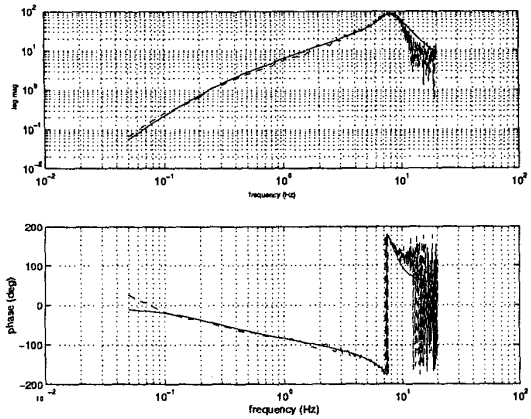

Fig. 3. Amplitude and phase Bode plot of frequency data $G(\omega)$ and curve fitted fourth-order model $\hat{G}(z^{-1}, \hat{\theta})$ (solid)

The estimated discrete time model is shown in a solid line on top of the measured frequency response $G(\omega)$ in Figure 3. The linear model $\hat{G}(q, \hat{\theta})$ is used to model the dynamics of the pneumatic positioning mechanism by considering the valve input voltage signal and the load acceleration signal. As the dynamic model is derived from a non-friction regime, the model $\hat{G}(q, \hat{\theta})$ will **simulate a non friction acceleration signal** $\hat{\ddot{x}}$ on the basis of a measured valve voltage input signal V_{in}. By comparing a measured acceleration signal $\ddot{x}$ with the simulated (friction free) acceleration signal $\hat{\ddot{x}}$, detection of friction faults can be accomplished.

IV. Friction Monitoring by Acceleration Measurements

A. Acceleration measurements and friction force

As was stated, detection of friction in a servo pneumatic application is desirable. In the detection scheme developed here, only the voltage input and measured and modelled accelerations of the air bearing mass are required to monitor the nonlinear dry friction force on-line for fault detection. The advantage of requiring the measurement of only acceleration is that inexpensive, reliable accelerometers are available and easily added to the load of a precision positioning apparatus.

A.1 Dynamic Relation Between Friction Force and Measured Acceleration

The non friction acceleration signal $\hat{\ddot{x}}(t)$ provides the non fault information with which the fault sensitive measurements, i.e. the measured acceleration $\ddot{x}(t)$, may be compared. As friction force is proportional to acceleration, it is intuitive that the difference in these signals would capture a friction fault in some way if it occurs. The acceleration residual is defined as

$$\ddot{x}_r \triangleq \ddot{x} - \hat{\ddot{x}}. \tag{3}$$

This signal alone can capture unmodeled faults such as dry friction. However, to achieve the fault detection and isolation objective, this signal must somehow be reduced to a signal or signals that are sensitive to friction faults and relatively robust to other possible sensor, actuation or process faults. To relate the friction force to this residual, a qualitative description about the behavior of simple dynamics with and without friction is helpful. Consider the linear system given by

$$m\,\ddot{x}_1 = F - k\,x_1 - c\,\dot{x}_1. \tag{4}$$

where x_1 represents the position, $\dot{x}_1$ the velocity and $\ddot{x}_1$ the acceleration of a mass m. When a dry friction force is present, the dynamics of the system in (4) change to

$$m\,\ddot{x}_2 = F - k\,x_2 - c\,\dot{x}_2 - F_f. \tag{5}$$

Subtracting (5) from (4) yields

$$m\,\ddot{x}_e + c\,\dot{x}_e + k\,x_e = -F_f, \tag{6}$$

where $\ddot{x}_e \triangleq \ddot{x}_1 - \ddot{x}_2$ is effectively an acceleration residual in (6). Therefore, (6) shows that a **dynamic relation** exists between the dry friction force F_f and the acceleration residual $\ddot{x}_e$. Clearly, these linear models do not represent the pneumatic cylinder and mass load dynamics with or without friction, but it does provide useful insight into a relation in the pneumatic cylinder experiment between friction and the acceleration residual. With this insight, it is left to model such a relation. First however, we must select a model for the friction force itself.

A.2 Proposed Friction Model

Most of the work that have addressed the compensation of friction in pneumatic actuator applications [3], [11] do not apply identification tools. According to Johnson and Lorenz, "...because of its nonlinear nature, friction is often neglected or inadequately compensated by conventional controllers" ([1], p.1392). Although friction has be compensated for by more modern control algorithms [1], sudden and unpredictable changes in friction due to, for example, wear and side loading of a pneumatic cylinder cause unacceptable behavior of the positioning mechanism.

For a dynamic system undergoing slipping dry friction, i.e. dry friction that has a comparatively low sticking and high slipping characteristic, the coulomb and viscous friction model has been validated in [12], [6], [13], with experimental validation in [14]. This model is therefore utilized here to capture the dry aluminum-on-aluminum sliding that occurs when the friction fault is induced in the experimental set-up. The friction model takes the form

$$F_f = \alpha\,\frac{\dot{x}}{|\dot{x}|} + \beta\,\dot{x}, \tag{7}$$

where only velocity measurements are needed. A third-order high pass digital Butterworth filter is used to eliminate any DC content in the measured acceleration signal and a discrete time integrator is used to compute the measured velocity. The chief advantage of this model is that it is linear in the parameters α and β and therefore facilitates identification. By recursively estimating these parameters with least-squares the friction fault level in the precision positioner is isolated and monitored for detection, as described in the next sections.

B. Estimation of friction coefficient changes

In Section IV-B.1, the filter that relates the friction force and the acceleration residual is detailed. A description of the process of estimating and monitoring the friction model parameters for fault detection is then given in Section IV-B.2.

B.1 Identification of Dynamic Friction Signal Filter

The dynamic model, or filter, between the friction force and the acceleration residual is written as an output error model [15], given as

$$y(t) = \left[B(q^{-1})/F(q^{-1})\right] u(t - nk) + e(t), \quad (8)$$

$$\text{where} \quad y(t) = \ddot{x}_r(t), \quad u(t) = F_f(t),$$

$$[nb,\ nf] = \left[\text{order of } B(q^{-1}),\ \text{order of } F(q^{-1})\right],$$

$$nk = \text{model delay order.} \quad (9)$$

and $e(t)$ represents the error between the acceleration residual and the filtered friction signal. The prediction error estimate of (8) finds the parameters in $B(q^{-1})$ and $F(q^{-1})$ that minimize the L_2 norm of $e(t)$, given $y(t)$ and $u(t)$. With these parameters, the dynamic filter simulates the acceleration residual for a given friction signal. Since friction lags the acceleration residual, the order of $B(q^{-1})$ is higher than that of $F(q^{-1})$. For this problem, the orders selected are $[nb,\ nf,\ nk] = [4,\ 3,\ 0]$.

B.2 Incorporation of Friction Model with Model Based Filter

Substituting (7) into (8) and normalizing the lead coefficient in the friction model yields,

$$\ddot{x}_r(t) = G_e(q^{-1}) \left[\frac{\dot{x}}{|\dot{x}|} + \gamma_f\ \dot{x}\right] + e(t) \quad (10)$$

$$= G_e(q^{-1})\ x_f(t) + e(t). \quad (11)$$

where $x_f(t)$ represents the friction signal after normalization of the coulomb term coefficient and the constant γ_f represents the relative amount of viscous to coulomb friction when the friction fault is present. It remains to estimate γ_f and G_e in the presence of a friction fault. A window of data in time, comprised of faulty acceleration measurements, computed velocities and modelled accelerations, define the signals in (10). Let the data window time interval be defined as $t \in [t_1, t_2]$. The parameter γ_f is iterated through the values $[0.0, 10.0]$ in steps of 0.2 and for each value, the parameters in G_e are estimated by least-squares with the cost function $e(t)$, i.e. the estimated parameters minimize

$$\left\| \ddot{x}_r(t) - G_e(q^{-1})\ x_f(t) \right\|_{L_2(t_1,t_2)}. \quad (12)$$

The set of G_e parameters and corresponding value of γ_f that result in the smallest $L_2(t_1, t_2)$ norm of the error $e(t)$ define, respectively, the dynamic filter and the relative level of viscous friction for the given window of data. Clearly then, for each servo voltage input and corresponding measured and modelled signals in which a friction fault occurs, a dynamic filter and associated level of viscous friction γ_f are generated. For this set of data, the filter parameters are fixed and the normalized friction model coefficients $(1,\ \gamma_f)$ serve as the signature values to which the recursively estimated friction model parameters are compared.

C. On-line implementation of friction detection

In this section a procedure is formulated for recursively estimating the friction model parameters and monitoring them for friction fault detection. Rewrite(10) in the form

$$\ddot{x}_r(t) = G_e(q^{-1}) \left[\frac{\dot{x}}{|\dot{x}|} + \gamma_f\ \dot{x}\right] + e(t)$$

$$= G_e(q^{-1}) \left[\frac{\dot{x}}{|\dot{x}|}\right] + \gamma_f\ G_e(q^{-1})\,[\dot{x}] + e(t), \quad (13)$$

where G_e and γ_f are defined. The normalized friction model coefficients $(1,\ \gamma_f)$ fit the filtered measured velocity signals in (13) to the acceleration residual in a least-squares sense. The fit is generated over a time domain window of data in which a friction fault is present. To fit filtered measured velocity signals to the acceleration residual signal on-line, these parameters can be estimated by least-squares using current windows of data, i.e. the parameters can be recursively estimated. Now the friction model coefficients are non-constant and are expected to vary slightly within and largely in transition between the non friction and friction regimes. To account for time varying coefficients, (13) is modified by

$$y(t) = \theta_1(t)\ g_1(t) + \theta_2(t)\ g_2(t) + e(t), \quad (14)$$

$$\text{where,} \quad y(t) = \ddot{x}_r(t),$$

$$g_1(t) = G_e(q^{-1}) \left[\frac{\dot{x}}{|\dot{x}|}\right],$$

$$g_2(t) = G_e(q^{-1})\,[\dot{x}],$$

and $\theta_1(t)$ and $\theta_2(t)$ represent the time varying coulomb friction and viscous friction coefficients, respectively. As was stated, these parameters ought to converge to their respective signature values $(1,\ \gamma_f)$ when the fault is present. These values indicate the relative level of Coulombic to viscous friction, respectively. Prior to the fault, the parameters match the small non friction acceleration residual and the filtered measured signals $g_1(t)$ and $g_2(t)$. As the fault is added over a window of time, the fit parameters in this transition are expected to display transient behavior that has no physical interpretation. The physical interpretation of the two parameters remains solely in their signature levels, exhibited when the fault is present and after some transient behavior. To implement the recursive estimation, (14) is rewritten as

$$y(t) = \boldsymbol{g}(t)^T \boldsymbol{\theta}(t) + e(t), \quad \text{where} \quad (15)$$

$$\boldsymbol{g}(t)^T = [\ g_1(t),\ g_2(t)\ ], \quad \boldsymbol{\theta}(t)^T = [\ \theta_1(t),\ \theta_2(t)\ ].$$

For a current window of $y(t)$ and $\boldsymbol{g}(t)$ data $t \in [t_a, t_b]$, the well known least-squares estimate $\hat{\boldsymbol{\theta}}(t_b)$ of the parameter vector $\boldsymbol{\theta}(t_b)$ at window time t_b is

$$\hat{\boldsymbol{\theta}}(t_b) = \left[\ \boldsymbol{g}(t)\ \boldsymbol{g}(t)^T\ \right]^{-1} \boldsymbol{g}(t)\ y(t), \quad t \in [t_a, t_b]. \quad (16)$$

The detection logic contains a non friction parameter value threshold level and compares the estimated parameters to the signature values. Simply, a fault is detected once the estimates exceed the thresholds and the parameters are monitored for tracking to the signature values. The parameters would likely exit the pre-fault threshold levels in the event of different types of faults. Successful tracking of the parameters to the signature values could therefore be considered as success in detection and isolation of the dry friction fault. The threshold levels are computed as the average plus and minus three times the standard deviation of an initial set of estimated parameter values $\hat{\boldsymbol{\theta}}$ that are known to be friction free.

A few words are in order about some properties of the parameter estimates. A property of recursive estimation of variables that are subject to random processes such as noise is that they exhibit variance. The variance is a function of the data batch length, the interval between data batches, and naturally the noise present in the batches themselves. Although the first two of these elements can be controlled in the detection scheme, the noise level cannot. Moreover, the signal noise levels are highly sensitive to varying input types and levels of friction, particularly in the experimental case. So, it is expected to observe different levels of parametric variance in the highly nonlinear system of the experiment for test cases that investigate varying input types, levels of friction, etc.

V. Experimental results

The FDI scheme has been numerically validated and seven different test cases display the success and limitations of the method described in the preceding sections when applied to the pneumatic cylinder and air bearing mass experiment [5]. These cases compare different levels of stiction in the friction fault for a range of voltage input signals. The wide range of inputs is applied to show that the scheme is not restricted to a specific input for success in detection and isolation of the friction fault. For brevity, two of these test case will be discussed and are displayed in Table I and Table II. Specifically, tests 1 and 2 compare different types of applied friction fault for common inputs.

TABLE I
Dry Friction Fault Detection Test Cases

Test	Input	Air Supply at the Fault
1	$1.4\sin(8 \times 2\pi t)$	slightly reduced supply
2	$1.5\sin(8 \times 2\pi t)$	completely cut-off supply

TABLE II
Dry Friction Fault Detection Test Cases

Test	Fault/Detection Time (sec)	Fault Character	(θ_1, θ_2) Performance
1	3.05/0.015	low stick high slip	well behaved
2	2.9/0.035	moderate stick high slip	well behaved

In Table I, air supply at the fault refers to the to the amount and speed that the air supply to the block is reduced to induce a friction fault. In Table II the fault character refers to the amount of sticking and slipping observed in the load acceleration measurements due to the friction fault. Fault occurrence time and detection time refer the time of initiation of the fault and of the parameters exiting their threshold windows, respectively. Parametric performance describes the behavior of the parameters prior to and after the fault. The parameters are "well behaved" when they track to a pre-friction level and to their signature values with little variance.

For the two test cases, all conditions are nearly equivalent (Voltage amplitude difference assumed negligible) except in the manner in which the friction fault is applied. Specifically, in case 1 the magnitude of the fault is smaller than in case 2. The measured acceleration and recursively estimated parameter evolution plots for test cases 1 and 2 are shown in Figure 4 and Figure 5, respectively. The occurrence of the fault in each case is marked in the acceleration plots in each figure. In the $\theta_1(t)$ and $\theta_2(t)$ plots,

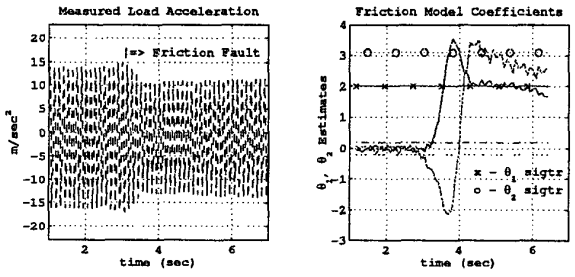

Fig. 4. Measured Acceleration and Friction Model Parameters for Test Case 1

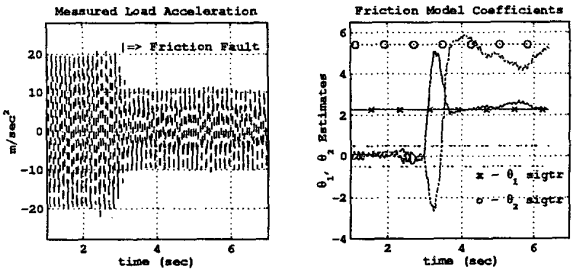

Fig. 5. Measured Acceleration and Friction Model Parameters for Test Case 2

the dashed lines represent the fault thresholds. These plots show a tracking time of 1.5 and 0.7 seconds, respectively, to the signature values with low variance. The value of $\theta_1(t)$ shows lower variance than that of $\theta_2(t)$ in both cases.

The measured acceleration shows a stiction effect in the peaks prior to the fault occurrence. For different voltage inputs, this effect varies and generally decreases for increasing input amplitude and frequency. In any case, the added dry friction fault is distinguished from any pre-fault stiction in the dynamic filter generation, thereby isolating the desired dry friction fault for detection. Although the estimated parameters have no physical meaning except by their signature values, they converge to this pre-fault stiction behavior.

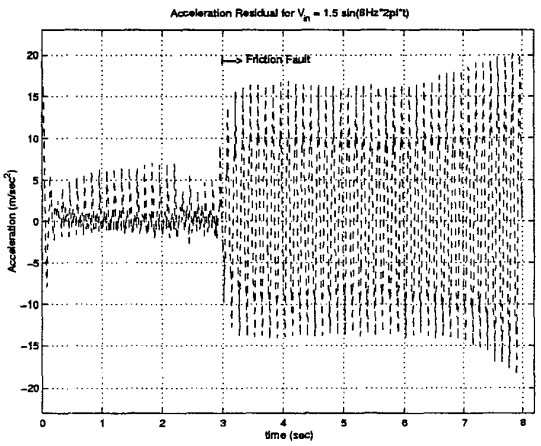

Fig. 6. Acceleration Residual for Test Case 2

It is useful to see how the parameter estimates are quantitatively related to measured acceleration. As discussed, the friction force is dynamically related to the difference between the measured and modelled accelerations, i.e. the acceleration residual, when friction is present. A plot of the acceleration residual for test case 2 is shown in Figure 6. As discussed in Section IV-B.1, the filter parameters and the signature values are estimated to fit the filtered friction model signal to this acceleration residual after the occurrence of the fault. In Figure 7, the fit between the filtered friction signal (solid) and the acceleration residual (dashed) shows the success of this approach. Thus, in the event of a fault the estimated parameters track to the parameter values that, with the estimated filter, generate a fit such as that exhibited in Figure 7.

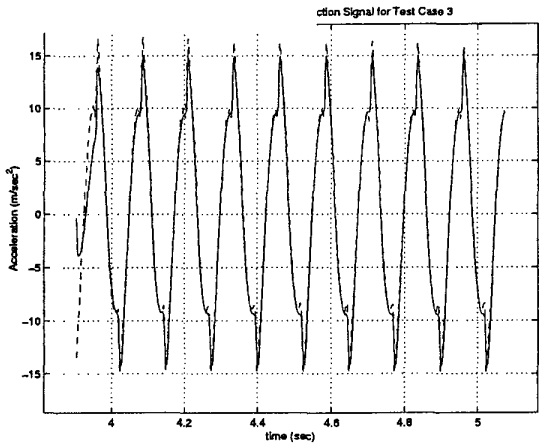

Fig. 7. Acceleration Residual (dashed) and Filtered Friction Model Signal (solid) for Test Case 2

VI. Conclusions

The fault detection scheme designed here detects changing process conditions in the case of wear and excessive side loading, in the form of dry friction, of a precision positioning device. A flow diagram of the implementation of this friction detection scheme is shown in Figure 8. The process input d represents noise present in the experimental apparatus, with or without friction. All other parameters and variables are defined in the previous sections.

By systematically reducing the data contained in the measured input (V_{in}) and output ($\ddot{x}$) signals to the estimation of two friction model parameter signals ($\hat{\theta}$), the scheme isolates the friction fault from other possible sensor, actuation or process faults that can occur in precision positioning devices. Thus, the goal of detection and isolation of FDI schemes has been achieved.

Experimental identification of friction and its compensation in precise, position controlled mechanisms was also investigated by Johnson and Lorenz [1]. Much like the scheme developed here, they utilize signal processing to expose a functional form of friction that they use for controlling an otherwise linear model. The work here adds the capability of detection of experimentally identified friction and has shown success in a highly nonlinear application, namely the pneumatic actuator. Moreover, the scheme is independent of any type of controller, suggesting use in conjunction with controllers of any form in these types of applications. There also exists freedom in the selection of the friction model in the scheme outlined here. Provided that the model depend linearly on the parameters, dependence upon other linear and nonlinear terms is also possible. In any case, a controls engineer would certainly benefit by applying this simple, reliable method of dry friction fault detection in lieu of or jointly with any precision compensation. For implementation in an experiment, the only added hardware required is an accelerometer, which is light-weight, inexpensive and easy to add to a positioned load.

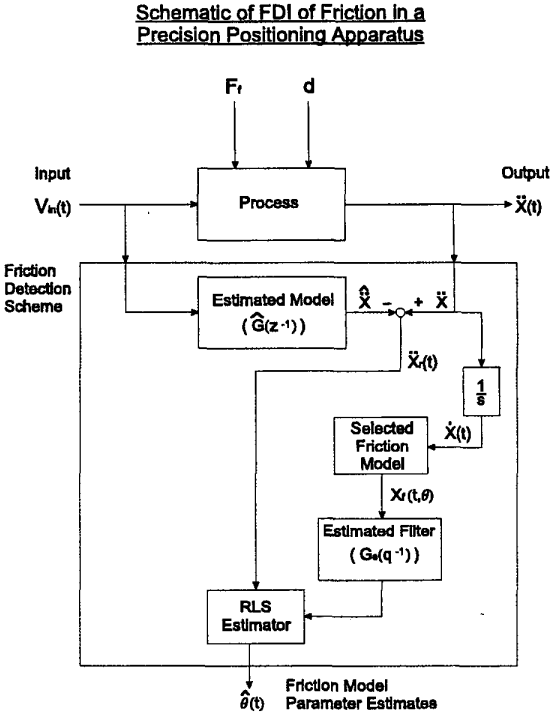

Fig. 8. Flow Diagram of Scheme for Fault Detection and Isolation of Dry Friction in a Precision Positioning Device.

References

[1] C. T. Johnson and R. D. Lorenz, "Experimental identification of friction and its compensation in precise, position controlled mechanisms," *IEEE Trans. Indus. Appl.*, vol. 28, no. 6, pp. 1392–1398, 1992.

[2] O. A. Johnson, *Fluid Power – Pneumatics*, American Technical Society, Chicago, 1975.

[3] J.-Y. Lai, C.-H. Menq, and R. Singh, "Accurate position control of a pnematic actuator," *Trans. ASME*, vol. 112, no. December, pp. 734–739, 1990.

[4] T. Nritsugu and M. Takaiwa, "Robust positioning control of pneumatic servo system with pressure control loop," *IEEE Inter. Conf. on Robotics and Automation*, pp. 2613–2618, 1995.

[5] W. B. Dunbar, "Damage detection in dynamic systems with nonlinearities," M.S. thesis, University of California, San Diego, 1999.

[6] P. E. Dupont and E. P. Dunlap, "Friction modeling and proportional-derivative compensation at very low velocities," *Trans. ASME*, vol. 117, no. 3, pp. 8–14, 1995.

[7] M.B. Priestley, *Spectral Analysis and Time Series*, Academic Press, London, England, 1981.

[8] R. A. de Callafon, D. Roover, and P. M. J. Van de Hof, "Multivariable least squares frequency domain identification using polynomial matrix fraction descriptions," *IEEE Conf. Dec. Conr.*, vol. June, pp. 2030–2035, 1996.

[9] R. A. de Callafon and P. M. J. Van de Hof, "Freqid – frequency domain identification toolbox for use with matlab," *Sel. Top. Iden. Modl. Conr.*, vol. 9, pp. 129–134, 1996.

[10] *MATLAB Application Program interface guide*, Natick, MA, 1998, ver. 5.

[11] S. R. Pandian, Y. Hayakawa, Y. Kanazawa, Y. Kamoyama, and S. Kawamura, "Practical design of a sliding mode controller for pneumatic actuators," *Trans. ASME*, vol. 119, no. December, pp. 666–674, 1997.

[12] C. Hatipoglu and U. Ozguner, "Robust control of systems involving non-smooth nonlinearities using modified sliding manifolds," *Proc. Amer. Contr. Conf.*, vol. June, pp. 2133–2137, 1998.

[13] D. A. Haessig Jr. and B. Friedland, "On the modeling and simulation of friction," *Proc. Amer. Contr. Conf.*, vol. 2, pp. 1256–1261, 1990.

[14] Y. S. Kang and K. J. Kim, "Friction identification in a sight stabilisation system at low velocities," *Mechanical Systems and Signal Processing*, vol. 11, no. 3, pp. 491–505, 1997.

[15] L. Ljung, *System Identification: Theory for the User*, Prentice Hall, New York, 1987.